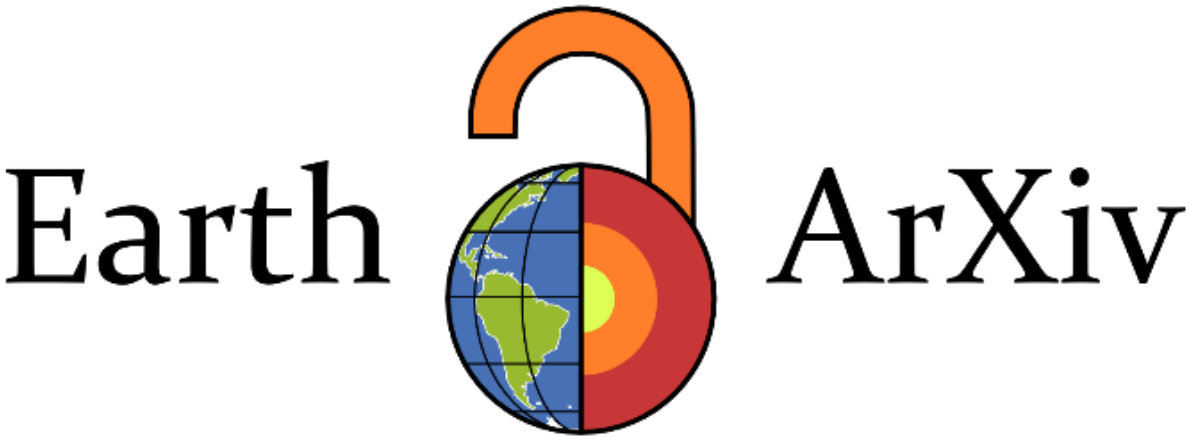


Peer review status:

This is a non-peer-reviewed preprint submitted to EarthArXiv.

Contrasting terrestrial and marine sources of isoprenoid and branched glycerol monoalkyl glycerol tetraethers in marine sediments

Jiaming Zhou[1]#, Jiale Liu[1]#, Xinming Yuan[1], Chenxi He[1], Lingjun Li[1], Yunru Chen[2], Binbin Guo[3], Zian Tong[1], Joanna J. Waniek[4], Yanwei Wang[1], Jing Zhao[3], Longhui Deng[1], Fengping Wang[1], Qianyong Liang[3], Liang Dong[1]*

[1] State Key Laboratory of Submarine Geoscience; Key Laboratory of Polar Ecosystem and Climate Change, Ministry of Education; Shanghai Key Laboratory of Polar Life and Environment Sciences; and School of Oceanography, Shanghai Jiao Tong University, 1954 Huashan Road, Shanghai 200030, China.
[2] MARUM–Center for Marine Environmental Sciences, University of Bremen, D-28359 Bremen, Germany.
[3] National Engineering Research Center of Gas Hydrate Exploration and Development, Guangzhou Marine Geological Survey, China Geological Survey, Guangzhou, 511457, China
[4] Leibniz Institute for Baltic Sea Research, Warnemünde, Rostock 18119, Germany.
#These authors contributed equally.

Corresponding author: Liang Dong (dongliang@sjtu.edu.cn).

Author email list:
Jiaming Zhou: zhoujiaming@sjtu.edu.cn
Jiale Liu: jialeliu@sjtu.edu.cn
Xinming Yuan: yxm3000@sjtu.edu.cn
Chenxi He: he.chen.xi@sjtu.edu.cn
Lingjun Li: llj_2261746391@sjtu.edu.cn
Yunru Chen: yunruchen@marum.de
Binbin Guo: guobinbin1990@hotmail.com
Zian Tong: sober123@sjtu.edu.cn
Joanna J. Waniek: joanna.waniek@io-warnemuende.de
Yanwei Wang: yanweiwang@sjtu.edu.cn
Jing Zhao: 79602738@qq.com
Longhui Deng: longhui.deng@sjtu.edu.cn
Fengping Wang: fengpingw@sjtu.edu.cn
Qianyong Liang: tolqy@163.com
Liang Dong: dongliang@sjtu.edu.cn

Abstract

Glycerol dialkyl glycerol tetraethers (GDGTs) are widely used as environmental proxies, yet the sources and environmental significance of the structurally related glycerol monoalkyl glycerol tetraethers (GMGTs) in marine sediments remain poorly constrained. We investigated isoprenoid and branched GMGTs in 16 coastal soils, 62 East China Sea surface sediments, five South China Sea sediment cores, and offshore suspended particles to distinguish terrestrial inputs from marine production. Isoprenoid GMGTs (isoGMGTs) occurred in coastal soils and declined across the shelf, with no detections in W07 particles or the offshore SCS cores. Elevated isoGMGTs/crenarchaeol ratios near the Yangtze River mouth and Hangzhou Bay resembled the published spatial pattern of the soil-derived bacteriohopanepolyol index R_{soil}, supporting their use as an indicator of soil organic matter input. Soil brGMGT assemblages contained nine resolved peaks, including three H1048 components, whereas among offshore samples with quantifiable brGMGTs, H1020a and H1020b accounted for >90% of the assemblage, with H1020c detected in some samples. H1020a and H1020b also constituted the quantifiable brGMGT assemblage in suspended particles at station W07, where concentrations peaked at 75 m in oxygenated waters. This correspondence supports a marine water-column contribution to sedimentary brGMGTs and indicates that their occurrence extends to oxygenated environments. The ratio H1020b/(H1020a + H1020b), expressed as IR_{H1020}, covaried inversely with TEX_{86} in all three offshore cores. These downcore variations may reflect glacial – interglacial environmental changes. Together, these findings support isoGMGTs/crenarchaeol as a tracer of relative soil organic matter input and identify a distinct marine brGMGT assemblage with potential for paleoceanographic applications.

Keywords: GMGTs; soil organic matter; terrestrial input; marine production; lipid composition; paleoenvironmental change

1. Introduction

Microbial tetraether lipids provide widely used tools for tracing organic matter sources and reconstructing environmental conditions in marine sediments (Dong et al., 2019; Dong et al., 2020; Summons et al., 2022; Zhou and Dong, 2024a; Zhou et al., 2026b). Archaeal isoprenoid glycerol dialkyl glycerol tetraethers (isoGDGTs) underpin the TEX_{86} paleothermometer (Kim et al., 2008; Kim et al., 2010; Schouten et al., 2002; Tierney and Tingley, 2015; Zhou and Dong, 2025), whereas bacterial branched GDGTs (brGDGTs) are widely used to reconstruct terrestrial temperature and pH (De Jonge et al., 2014; Peterse et al., 2012; Raberg et al., 2022; Weijers et al., 2007). Marine brGDGT production, including that documented in oceanic suspended particles, further demonstrates that terrestrial delivery and marine production can contribute to the same sedimentary lipid assemblage (Xiao et al., 2016; Zhou et al., 2026c). Compared with GDGTs, the sources and environmental significance of the structurally related glycerol monoalkyl glycerol tetraethers (GMGTs) remain much less understood in marine settings. In particular, the contributions of terrestrial inputs and marine production to sedimentary GMGT distributions have yet to be systematically resolved.

GMGTs, also termed H-shaped GDGTs, contain an additional covalent C–C bond linking their alkyl chains (Fig. S1) (Liu et al., 2012; Morii et al., 1998). Isoprenoid GMGTs (isoGMGTs) were first characterized in the hyperthermophilic methanogen *Methanothermus fervidus* and subsequently reported from hydrothermal chimneys and terrestrial hot springs (Jia et al., 2014; Lincoln et al., 2013). These occurrences motivated a thermal-adaptation interpretation, supported by molecular dynamics simulations showing that H-bridging increases membrane packing and reduces permeability (Zhou and Dong, 2024b). Recent identification of archaeal GMGT-biosynthesis proteins, together with increased GMGT production at elevated growth temperatures in two *Archaeoglobus* species, provides experimental support for temperature-sensitive biosynthesis (Garcia et al., 2024). The distribution of putative Gms homologs among anaerobic archaea and oxygen-deficient metagenomes also suggests an association with oxygen availability (Li et al., 2024), while culture responses to pH and salinity indicate broader physiological controls on GMGT production (Tourte et al., 2022).

Research on branched GMGTs (brGMGTs) has advanced particularly rapidly in terrestrial and freshwater environments. Their occurrence in peats, lakes, and rivers reveals diverse assemblages and environmental relationships (Baxter et al., 2019; Baxter et al., 2021; Kirkels et al., 2022; Naafs et al., 2018; Zhang et al., 2024). Positive associations with temperature in global peats and East African lake sediments underpin their development as terrestrial

paleothermometers (Baxter et al., 2019; Naafs et al., 2018), with applications to late Quaternary peat sequences, Late Miocene deposits in the Xining Basin, and Plio-Pleistocene fluvial–lacustrine sediments in northern China (Huang et al., 2024; Qian et al., 2025; Shen et al., 2025; Tang et al., 2021). These studies also highlight the importance of production habitats. Anoxic production in Lake Chala waters and surface sediments (Baxter et al., 2021), compositional changes along estuarine salinity gradients (Zhang et al., 2024), and contrasting environmental controls in lake surface sediments and downcore records (Wu et al., 2025) demonstrate that producer ecology contributes to sedimentary brGMGT variability. Carbon isotope evidence further supports heterotrophic bacterial sources and distinct contributions to the brGMGT and brGDGT pools (Elling et al., 2023). Understanding the origins of these lipids is therefore central to interpreting their environmental signals.

Marine GMGT research remains comparatively limited. Although brGMGTs have been reported from marine sediments and oceanic oxygen minimum zones (Liu et al., 2012; Xie et al., 2014), their distributions across terrestrial source materials, marine particles, and sedimentary archives remain sparsely documented. Existing studies provide important indications of source differentiation. IsoGMGTs/crenarchaeol was proposed as a potential indicator of terrestrial input based on its association with bulk organic matter composition in nearshore South China Sea sediments (Zhou et al., 2026a). For brGMGTs, enrichment of H1020a and H1020b in a Holocene Bay of Bengal core relative to the Godavari Basin suggested a marine contribution (Kirkels et al., 2022), while compositional changes along the Seine Estuary indicated source differentiation during river-to-sea transport (Zhang et al., 2024). A systematic comparison of terrestrial materials, marine particles, and sediments is needed to connect these observations and establish how source differences are expressed in marine sedimentary records. Such comparisons can also clarify the environmental settings in which GMGTs occur and provide a basis for evaluating their geochemical applications.

Here we investigate isoprenoid and branched GMGTs in 16 coastal soils, 62 Yangtze River Estuary and East China Sea surface sediments, five South China Sea sediment cores, and suspended particulate matter (SPM) from offshore station W07. High-resolution tandem mass spectrometry supports compound assignments, including three resolved H1048 components. By integrating soil, shelf, water-column, and sediment-core observations, we evaluate isoGMGTs as tracers of soil organic matter input and identify compositional signatures of marine brGMGT contributions. We then examine these source relationships in the context of proposed temperature and oxygen controls and assess variability within the dominant marine

H1020 pair through comparison with TEX_{86} records. This approach links GMGT sources and production environments to their sedimentary expression, providing a foundation for their use in marine organic geochemistry and paleoceanography.

2. Materials and Methods

2.1. Sample collection

2.1.1. Surface sediments from the Yangtze River Estuary and East China Sea

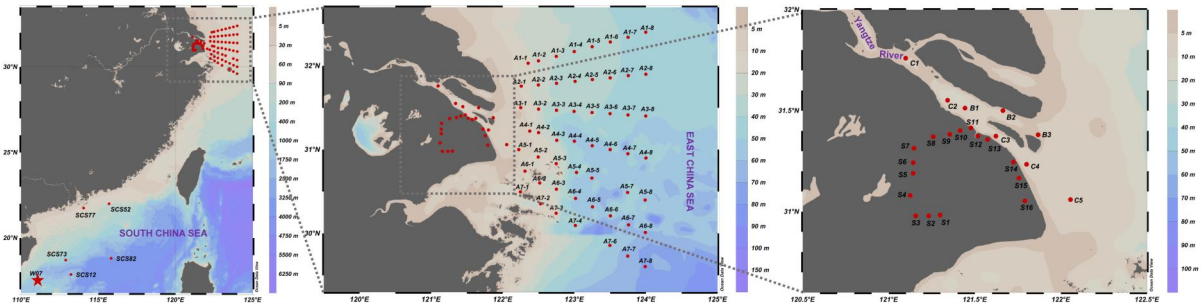


Fig. 1. Locations of surface sediment and soil samples in the Yangtze River Estuary and East China Sea, the five sediment cores in the northern South China Sea, and water-column station W07. Colors indicate water depth.

Surface sediments were collected at 62 stations in the Yangtze River Estuary and East China Sea (ECS) during the winter NORC2025-03 cruise supported by the National Natural Science Foundation of China. The stations covered estuarine channels and seven offshore transects (A1–A7), spanning water depths of 7–73 m (Fig. 1). Sediments were recovered using a 0.25 m^2 box corer or a Van Veen grab sampler, stored at −20 °C, and freeze-dried before lipid extraction.

2.1.2. Sediment cores and suspended particles from the South China Sea

Five northern South China Sea (SCS) sediment cores, SCS77, SCS52, SCS73, SCS12, and SCS82, were collected during R/V SONNE cruise SO269 in August–September 2019 (SOCLIS project, funded by the German Federal Ministry of Education and Research, BMBF, grant 03G0269) and span shelf to basin settings (Fig. 1). SCS77 and SCS52 form the nearshore group, and SCS73, SCS12, and SCS82 the offshore group. Published isoGMGT and GDGT measurements are compared here with new brGMGT analyses (Zhou et al., 2026a). Regional sedimentation rates and age constraints from nearby published records provide an approximate temporal context. The records are presented against sediment depth.

SPM was collected at station W07 (17.6224°N, 111.0548°E; water depth 1770 m) in the northern South China Sea during the HYDZ2-202410 cruise in November 2024 (Zhou et al., 2026c), at 5, 75, 200, 1000, and 1740 m. The same station was reported as oxygenated in Zhou et al. (2026c). Sampling procedures and isoGDGT and brGDGT measurements were reported

by Zhou et al. (2026c). We analyzed GMGTs in the same extracts to compare water-column concentrations and compositions with sedimentary assemblages.

2.1.3. Coastal soils

Sixteen surface soils (S1–S16) were collected in July 2026 from coastal areas adjacent to the ECS at 30°58′–31°24′N and 121°7′–121°47′E (Fig. 1). The upper 0–10 cm was collected into polyethylene bags and stored at −20 °C. These soils provide a local terrestrial reference for the adjacent shelf sediments.

2.2. Lipid extraction and analysis

2.2.1. Lipid extraction

Approximately 2 g of freeze-dried, homogenized ECS sediment or coastal soil was extracted by ultrasonication with dichloromethane/methanol (5:1, v/v) in five successive cycles. A known amount of synthetic C_{46} glycerol trialkyl glycerol tetraether (GTGT) was added before extraction as an internal standard (Huguet et al., 2006). The combined supernatants were filtered through glass wool and concentrated under nitrogen.

SCS sediment extraction followed the published procedure (Zhou et al., 2026a). W07 extracts were prepared following the published protocol (Zhou et al., 2026c): one aliquot was analyzed directly for core lipids (CLs), and a second was hydrolyzed to measure total lipids (TLs), including CLs and lipids released from hydrolysable polar precursors. GMGTs were analyzed in both aliquots, and CL and TL distributions are reported separately.

2.2.2. Chromatography and mass spectrometry

GMGTs and GDGTs were analyzed with an Agilent 1260 Infinity liquid chromatograph coupled to a Bruker Impact II quadrupole time-of-flight mass spectrometer equipped with an atmospheric pressure chemical ionization source (LC–APCI–QTOF–MS). Two Waters Acquity BEH HILIC amide columns (1.7 μm, 2.1 × 150 mm) were connected in series and held at 50 °C. The flow rate was 0.4 mL min^{-1}. Eluent A was n-hexane, and eluent B was n-hexane/isopropanol (90:10, v/v). The gradient began at 10% B for 10 min, increased linearly to 35% B over 15 min and to 100% B over the next 15 min, and remained at 100% B for 5 min. The system then returned to 10% B over 10 s and equilibrated for 10 min.

Mass spectra were acquired in positive-ion mode over m/z 100–2000. The APCI settings were a capillary voltage of 4000 V, an endplate offset of −500 V, a nebulizer pressure of 2.5 bar, a drying gas flow of 2.5 L min^{-1} at 250 °C, and a vaporizer temperature of 400 °C. Tandem mass spectra (MS^2) were obtained by collision-induced dissociation at 35–50 eV.

GMGTs were assigned using retention behavior, exact precursor masses, and diagnostic MS^2 fragments (Baxter et al., 2019; Liu et al., 2012; Naafs et al., 2018), with environmental reference extracts, including peat, used for chromatographic comparisons. Diagnostic fragmentation distinguished GMGTs from near-coeluting signals at nominal m/z 1300 with GDGT-like spectra (Zhou et al., 2026a). Representative spectra are shown in Fig. S2. Concentrations were semi-quantified against the C46 GTGT internal standard. Soil and sediment concentrations are expressed per gram of dry sample, and SPM concentrations per liter of filtered seawater.

2.3. Lipid indices

IsoGMGTs/CREN was calculated as the concentration of the identified GMGT-0 signal at nominal m/z 1300 divided by the crenarchaeol concentration (CREN; nominal m/z 1292), following the published definition (Zhou et al., 2026a). Here, isoGMGTs denotes the targeted isoGMGT-0 peak set. GDGT-0/CREN was also used to compare archaeal lipid source composition among the soils.

The relative abundance of brGMGTs, %brGMGTs, was calculated as 100 × ΣbrGMGTs/(ΣbrGMGTs + ΣbrGDGTs), following the relative-abundance approach of Naafs et al. (2018). The brGMGT sum includes the nine resolved peaks in this study. Fractional abundances of individual brGMGTs were normalized to this sum. The same definitions were applied separately to CL and TL fractions.

Because H1020a and H1020b dominate offshore brGMGT assemblages, their relative contributions were described by the H1020 component ratio, IR_{H1020}:

$$IR_{\mathrm{H1020}} = \frac{[\mathrm{H1020b}]}{[\mathrm{H1020a}] + [\mathrm{H1020b}]} \quad (1)$$

Square brackets denote concentrations. IR_{H1020} ranges from 0 to 1 and increases with the contribution of H1020b to the H1020a/b pool. Published TEX_{86} values (Zhou et al., 2026a) were compared with brGMGT indices at corresponding sediment horizons.

2.4. Statistical analysis

Principal component analysis (PCA) of the fractional abundances of the nine brGMGT peaks summarized compositional differences among sample groups. Linear regressions of %brGMGTs and IR_{H1020} against TEX_{86} were calculated for each SCS core and for the pooled dataset. We report coefficients of determination (R^2) and unadjusted p values. Separate within-core and pooled analyses distinguish stratigraphic covariation from the combined spatial and stratigraphic structure of the dataset.

3. Results

3.1. IsoGMGTs in soils and marine samples

IsoGMGTs occurred in coastal soils and ECS surface sediments (Fig. 2A). Most soil concentrations were approximately 0.2–1.1 ng g^{-1}, with some samples below detection and a maximum of approximately 3.7 ng g^{-1}. Soil GDGT-0/CREN values were below 2 except S4 (GDGT-0/CREN = 4.2); isoGMGT abundance was also relatively low at S4. The median isoGMGT concentration in ECS sediments was approximately 0.4 ng g^{-1}. Published nearshore SCS concentrations were approximately 0.7–2.6 ng g^{-1}, with a median of approximately 1.4 ng g^{-1}, whereas isoGMGTs were not detected in the three offshore cores (Zhou et al., 2026a).

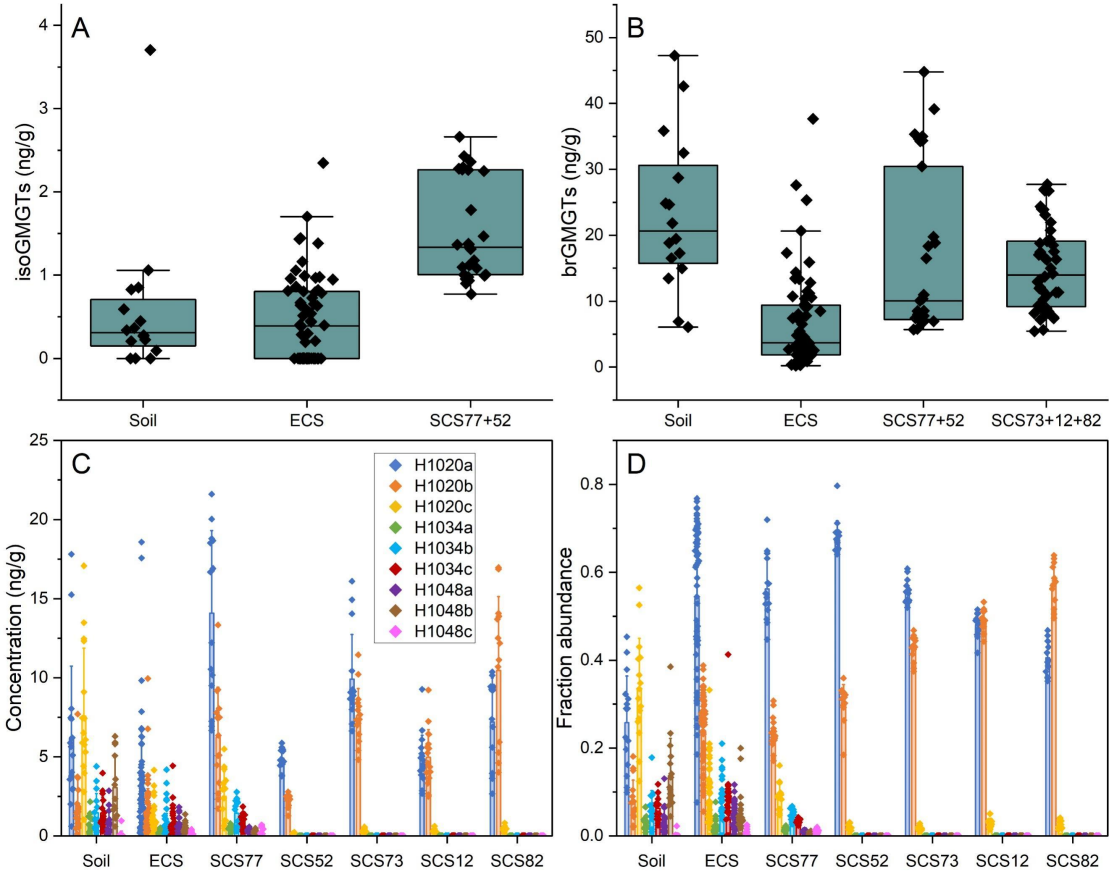


Fig. 2. GMGT concentrations and compositions in coastal soils, ECS surface sediments, and SCS sediment cores. (A) IsoGMGT concentrations. (B) Total brGMGT concentrations. (C) Individual brGMGT concentrations. (D) Fractional abundances of the nine brGMGT components. Nearshore cores are SCS77 and SCS52; offshore cores are SCS73, SCS12, and SCS82. SCS isoGMGT data are from Zhou et al. (2026a); brGMGT data are from this study.

In the ECS, isoGMGT concentrations were generally higher near the river mouth and lower on the outer shelf, with local maxima interrupting the offshore decline (Fig. 3A). IsoGMGTs/CREN ranged from approximately 0 to 0.0065, with high values near the Yangtze River mouth and Hangzhou Bay and generally lower values on the outer shelf (Fig. 3B). At W07, isoGMGTs were not detected at all five sampled depths between 5 and 1740 m.

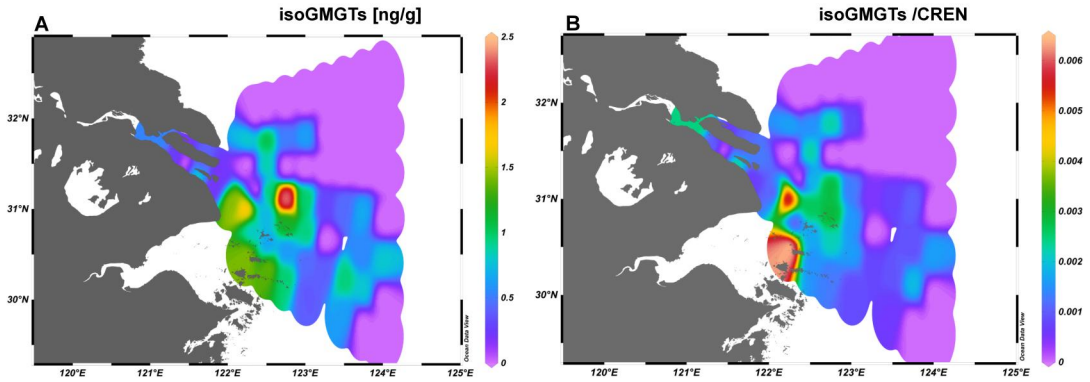


Fig. 3. Spatial distributions of (A) isoGMGT concentrations and (B) isoGMGTs/CREN ratios in surface sediments of the Yangtze River Estuary and East China Sea.

3.2. BrGMGT diversity and composition

Nine chromatographic peaks were assigned to brGMGTs in the soil extracts (Fig. 4A). The H1048, H1034, and H1020 homologues eluted at approximately 29.9–30.6, 30.5–31.2, and 31.0–31.6 min, respectively, with three chromatographic components in each homologue designated a, b, and c in order of elution. Exact precursor masses and diagnostic fragments supported the H1048 assignments (Fig. S2). H1020 and H1034 nomenclature followed the established chromatographic order (Baxter et al., 2019).

Median total brGMGT concentrations were approximately 20 ng g^{-1} in coastal soils, 4 ng g^{-1} in ECS surface sediments, 10 ng g^{-1} in the nearshore SCS cores, and 14 ng g^{-1} in the offshore cores (Fig. 2B). Concentrations in both nearshore and offshore SCS sediments exceeded those in ECS surface sediments.

BrGMGT composition differed among environments (Figs. 2C, 2D). All nine peaks occurred in the soil dataset, with substantial contributions from H1020c and the H1034 and H1048 homologues. In ECS sediments, H1020a reached a fractional abundance of approximately 0.78, and H1020b contributed 0.2–0.4. SCS77 retained a diverse assemblage, whereas SCS52 was dominated by H1020a and H1020b. In the three offshore cores, H1020a and H1020b together accounted for more than 90% of total brGMGTs; H1020c was detected in only some samples.

3.3. Spatial distributions of brGMGTs in the East China Sea

Total brGMGT concentrations were elevated off the Yangtze River mouth and in the northeastern part of the study area (Fig. 4B). Lower concentrations occurred in the estuarine channels, along much of the Zhejiang coast, and across the outer shelf. H1020a and H1020b had the broadest distributions and largely accounted for the spatial pattern in total brGMGT

concentrations (Fig. 4C). H1020c and the H1034 and H1048 homologues were concentrated closer to the estuary, although their local maxima differed.

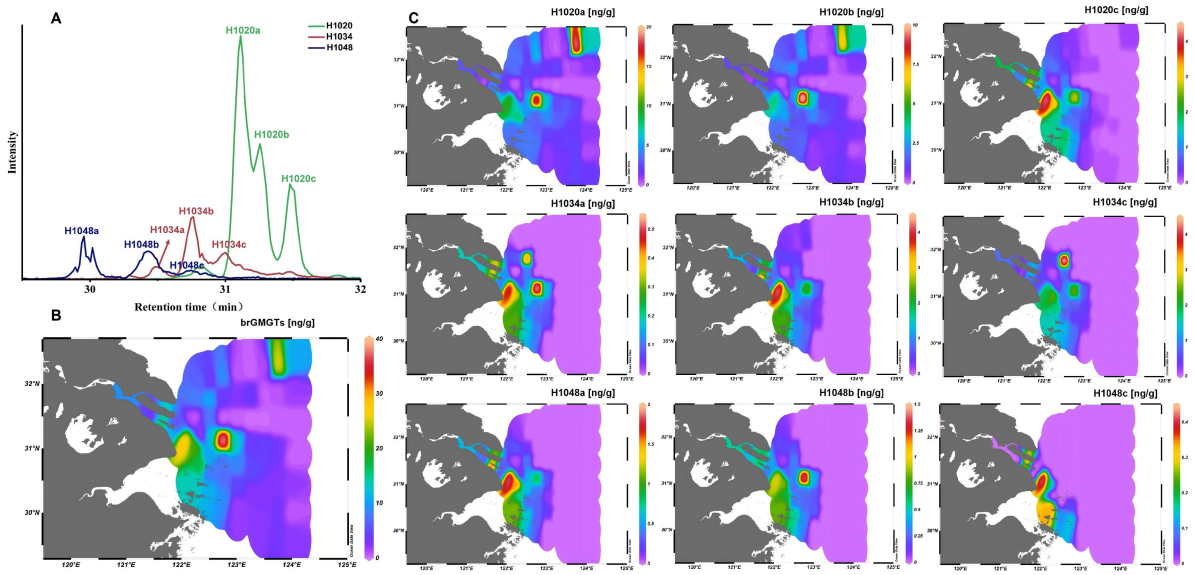


Fig. 4. Chromatographic separation and concentrations of brGMGTs. (A) Representative chromatogram showing the nine assigned brGMGT peaks. (B) Total brGMGT concentrations in ECS surface sediments. (C) Concentrations of the individual brGMGT isomers in the sediments.

The fractional abundance of H1020a increased from approximately 0.1–0.2 in the estuary to 0.6–0.8 on the outer shelf (Fig. 5). H1020b ranged from approximately 0.05 to 0.4, with a weaker offshore increase. H1020c reached approximately 0.3–0.35 in estuarine channels and declined seaward. The H1034 and H1048 compounds contributed mainly to estuarine and nearshore assemblages and their contribution was minor offshore.

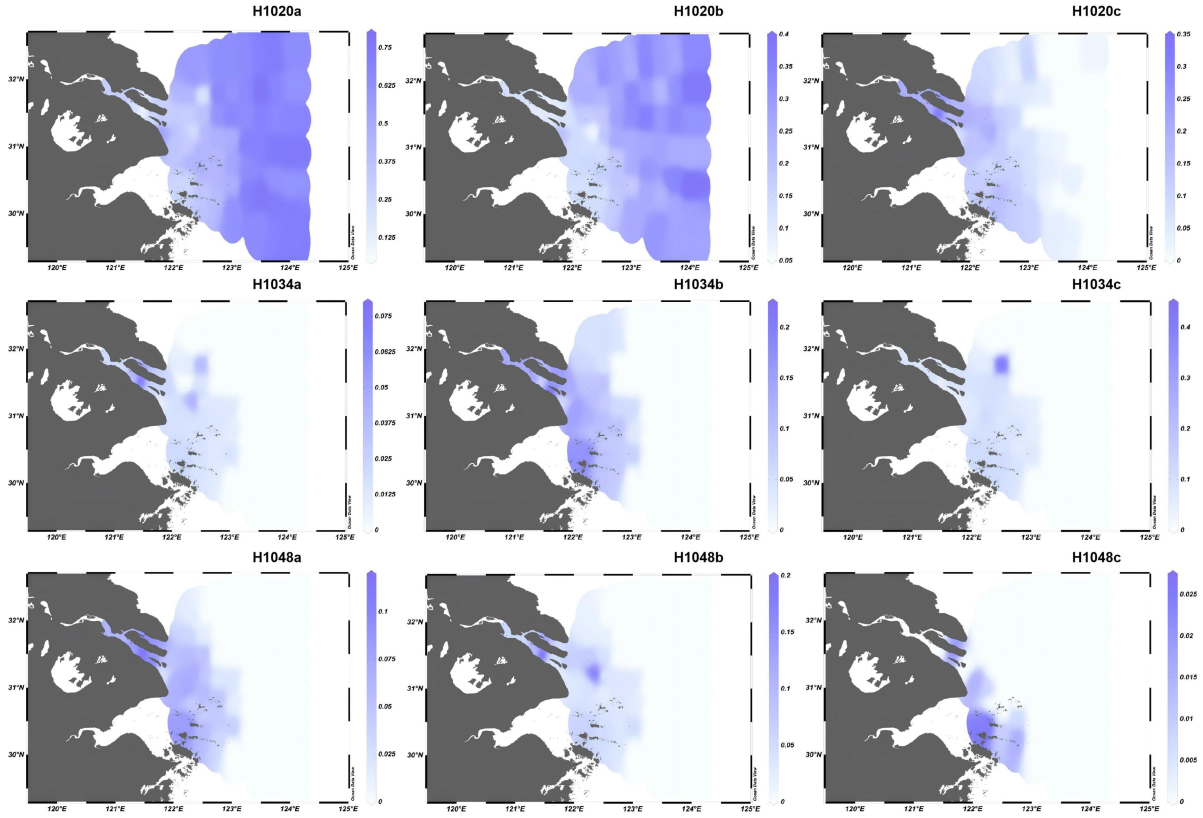


Fig. 5. Fractional abundances of the nine brGMGT components in surface sediments of the Yangtze River Estuary and East China Sea. Each fraction is normalized to total brGMGTs.

Values of %brGMGTs were generally low in estuarine channel and Zhejiang coastal sediments and higher in the northeastern ECS and locally off the river mouth (Fig. 6A). IR_{H1020} showed a heterogeneous distribution, with elevated values locally near the estuary and no consistent offshore gradient (Fig. 6B). This spatial pattern differed from the pronounced seaward increase in the combined contribution of H1020a and H1020b to total brGMGTs.

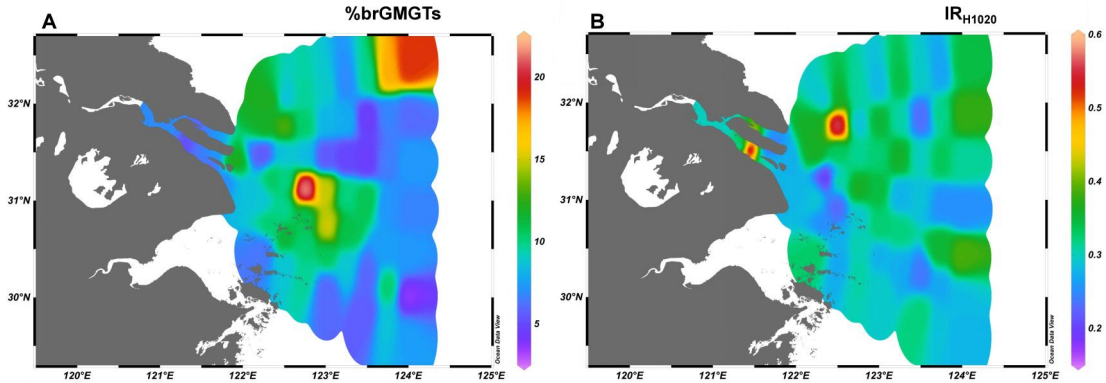


Fig. 6. Spatial distributions of (A) %brGMGTs and (B) IR_{H1020} in surface sediments of the Yangtze River Estuary and East China Sea.

3.4. BrGMGTs in the W07 water column

Both CL and TL brGMGT concentrations reached a maximum at 75 m and were lower in deeper samples (Fig. 7A). This maximum coincided with that in the previously reported

brGDGT profile (Zhou et al., 2026c). BrGMGTs were not reliably quantifiable at 5 m, and CL-brGMGTs were below reliable quantification at 1000 m.

All quantifiable W07 brGMGT assemblages consisted of H1020a and H1020b (Fig. 7B). H1020a accounted for 58%–66% of CL-brGMGTs and 56%–73% of TL-brGMGTs. In the TL fraction, its contribution was greatest at 1000 m and lowest at 1740 m. Values of %brGMGTs were approximately 14%–22% across the quantifiable samples and showed no monotonic depth trend.

3.5. Multivariate differences in brGMGT composition

PC1 and PC2 explained 60.88% and 13.97% of the variance in brGMGT fractional abundances, respectively (Fig. 8). H1020a and H1020b had negative PC1 loadings, and the three offshore SCS cores clustered at negative PC1 scores. Most soils had positive PC1 scores, while ECS sediments spanned a broad range along this axis. H1048c and H1034b had positive PC2 loadings, whereas H1020c, H1034a, and H1048b had negative PC2 loadings. SCS77 extended toward positive PC1 and PC2 scores; SCS52 plotted closer to the offshore cores.

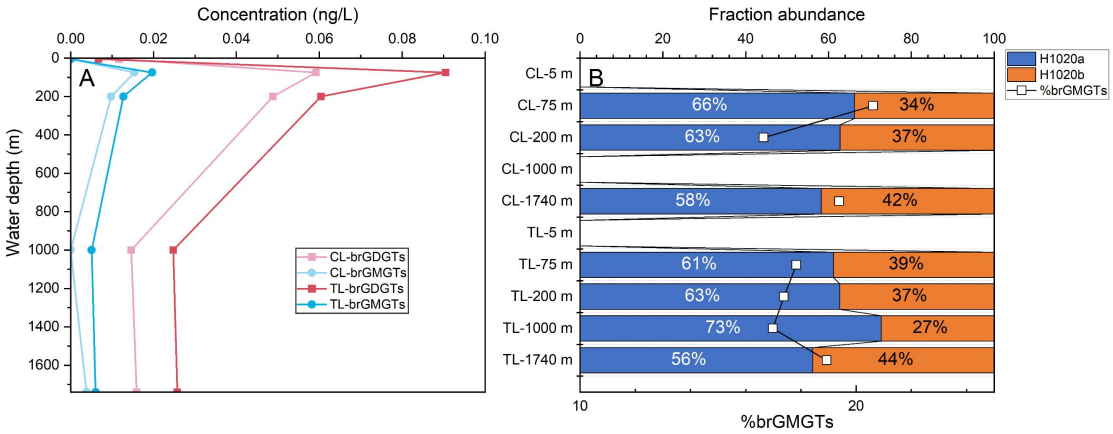


Fig. 7. Tetraether lipid distributions in SPM at W07 in the northern South China Sea. (A) BrGDGT and brGMGT concentrations in core lipid (CL) and total lipid (TL) fractions. (B) Fractional abundances of H1020a and H1020b (bars, upper axis) and %brGMGTs (squares, lower axis). BrGDGT data are from the published record (Zhou et al., 2026c); brGMGT data are from this study.

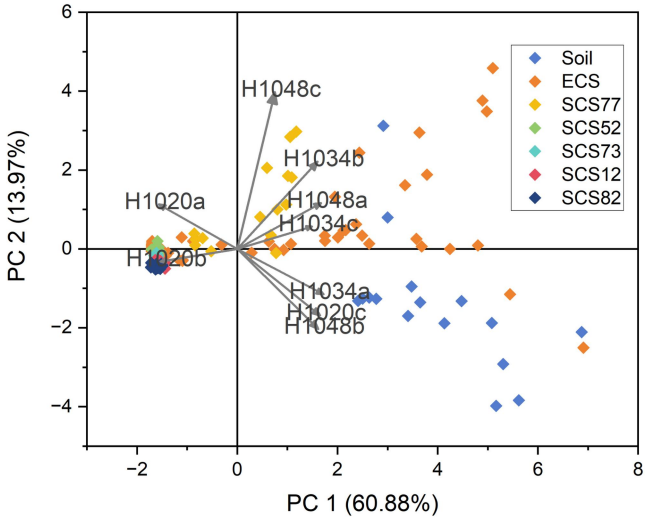


Fig. 8. PCA of brGMGT fractional abundances in soils, ECS surface sediments, and SCS sediment cores. Symbols represent samples, and arrows show component loadings. PC1 and PC2 explain 60.88% and 13.97% of the variance, respectively.

4. Discussion

4.1. Soil organic matter input recorded by isoGMGTs

Coastal soils provide direct evidence for a terrestrial isoGMGT source to adjacent marine sediments. The relationship between nearshore SCS GMGT-0 and bulk organic matter composition previously suggested a terrestrial contribution (Zhou et al., 2026a). Their detection in most of the 16 coastal soils establishes a local soil lipid pool, extending the documented terrestrial occurrence beyond peat (Naafs et al., 2018). The offshore decline in both concentrations and isoGMGTs/CREN across the ECS shelf (Figs. 2A, 3) is consistent with dispersal and dilution of this soil-derived material.

IsoGMGTs have been reported from marine and lacustrine sediments (Schouten et al., 2008), and the phylogenetic distribution of Gms indicates diverse potential producers (Garcia et al., 2024; Li et al., 2024). Here, diagnostic MS^2 fragmentation supports assignment of the targeted isoGMGT signal (Zhou et al., 2026a), while its occurrence in soils and nearshore sediments, together with its absence from W07 particles and offshore SCS cores, defines a coherent land-to-sea distribution. This combination of source and spatial evidence supports soil input as a major regional contributor.

The isoGMGTs/CREN distribution closely resembles published R_{soil} patterns, including high values near both the Yangtze River mouth and Hangzhou Bay (Fig. S3B). R_{soil} expresses soil-marker bacteriohopanepolyols relative to their sum with bacteriohopanetetrol (Zhu et al., 2011a). Agreement between these archaeal and bacterial biomarkers strengthens the interpretation of a soil organic matter signal. Other terrestrial markers trace different organic

matter components: leaf waxes (Eglinton and Eglinton, 2008) and lignin (Hedges and Mann, 1979) occur in vascular-plant debris as well as reworked soil organic matter, while aquatic production contributes to shelf tetraether assemblages (Zhu et al., 2011b). In the ECS, soil-marker BHP concentrations attenuate more rapidly offshore than plant-wax *n*-alkanes, reflecting differences in organic matter composition, reactivity, mineral association, and hydrodynamic sorting (Fig. S3A) (Zhu et al., 2011a). These component-specific differences help explain why isoGMGTs/CREN can follow R_{soil} while differing from other indicators of terrestrial input.

Normalization to crenarchaeol expresses soil-derived isoGMGT abundance relative to a predominantly marine archaeal lipid pool (Sinninghe Damsté et al., 2002). The soil detections, shelf gradient, and resemblance to R_{soil} extend the nearshore SCS interpretation (Zhou et al., 2026a) and support isoGMGTs/CREN as a relative indicator of soil-associated organic matter input to continental-margin sediments.

4.2. Sources of terrestrial and marine brGMGT assemblages

BrGMGT assemblages show a compositional contrast consistent with different source mixtures across the present dataset (Figs. 2, 5, 8). Soils contain nine resolved peaks, including appreciable H1020c, H1034, and H1048 components, whereas H1020a and H1020b account for more than 90% of brGMGTs in all three offshore SCS cores. A previous Holocene core from the Bay of Bengal showed enrichment of H1020a/b relative to the Godavari Basin, which suggested a marine contribution (Kirkels et al., 2022). Here, the recurrence of an H1020a/b-dominated assemblage across three offshore cores, together with direct comparisons with coastal soils, supports a distinct marine contribution. Nearshore SCS sediments contain different mixtures: SCS77 retains a diverse, soil-like assemblage, while SCS52 more closely resembles the offshore group.

Riverine and estuarine processes can further modify the terrestrial contribution. In the Godavari basin, brGMGT occurrence in inundated soils and river sites receiving nutrient-rich effluents suggests aquatic production (Kirkels et al., 2022). Along the Seine Estuary, H1020a/b enrichment accompanies increasing salinity, whereas H1020c and H1034b are associated with freshwater conditions (Zhang et al., 2024). Aquatic production and selective loss likewise modify brGDGT assemblages between the Yenisei River and Kara Sea (De Jonge et al., 2015). The progressive offshore enrichment of H1020a/b in the ECS is therefore consistent with increasing marine contributions superimposed on soil and riverine inputs.

The W07 observations connect this offshore sedimentary assemblage to a water-column particle pool. H1020a and H1020b are the only quantifiable brGMGT components in SPM, and both CL and TL concentrations peak at 75 m, coinciding with the previously reported brGDGT maximum (Zhou et al., 2026c) (Fig. 7). Earlier oceanic particle measurements detected H1020 in an eastern tropical Pacific oxygen minimum zone (Xie et al., 2014). In the Bay of Bengal, a deep-water or sedimentary source was inferred from sediment composition and lake-calibrated brGMGT temperature estimates (Kirkels et al., 2022). W07 identifies the H1020a/b pair directly in oxygenated water-column particles and links its subsurface maximum to the composition preserved in multiple offshore cores. This correspondence supports a marine contribution to the offshore assemblage and identifies a subsurface contribution.

The three chromatographic H1048 components add compositional detail to the seven-component brGMGT assemblage commonly reported from East African lakes (Baxter et al., 2019). H1048 was below reliable detection in the Bay of Bengal record (Kirkels et al., 2022), whereas its occurrence here is concentrated in soils and nearshore sediments. Exact precursor masses and diagnostic MS^2 fragments support the assignments (Fig. S2). The distinct ECS distributions and PCA loadings of the three peaks (Figs. 4, 5, 8) indicate heterogeneity within the terrestrial and nearshore brGMGT pools. The H1048 labels a, b, and c identify chromatographic components in elution order. Their contrasting distributions are consistent with the ecological differentiation proposed for other brGMGT components (Baxter et al., 2024). Resolving these components preserves source information that is combined when H1048 is reported as a single peak.

The predominance of H1020 and scarcity of the more highly methylated H1034 and H1048 homologues in offshore assemblages may reflect differences in bacterial producers or physiological adaptation between terrestrial and marine environments. Differences in salinity and organic substrate availability could influence both community composition and membrane lipid biosynthesis. Resolving their respective contributions will require paired lipid and microbial community analyses across environmental gradients, complemented by culture experiments. The co-occurrence of brGMGTs and brGDGTs in the W07 water column, together with their coincident subsurface maxima, is consistent with overlapping bacterial sources or shared ecological requirements. Their sedimentary distributions offer different opportunities for source discrimination. Although marine production of brGDGTs is increasingly recognized, separating terrestrial and marine contributions remains challenging (Zhou et al., 2026c). In the present dataset, the contrast between diverse soil brGMGT assemblages and H1020a/b-dominated offshore assemblages provides a clearer compositional

basis for recognizing marine contributions. This distinction may help identify marine-derived lipid signals and strengthen their potential for paleoceanographic reconstruction.

4.3. Temperature and oxygen controls on GMGT distributions

Temperature can influence GMGT distributions through membrane adaptation and producer ecology. GMGT synthase provides the enzymatic basis for archaeal H-bridge formation, and culture studies demonstrate temperature-sensitive GMGT production (Garcia et al., 2024; Li et al., 2024; Tourte et al., 2022). Molecular dynamics simulations show that the additional C–C bond increases membrane packing and reduces fluidity and permeability (Zhou and Dong, 2024b), providing a physical basis for increased H-bridging at elevated temperature. Environmental responses vary among habitats: isoGMGT abundance and cyclization respond differently to temperature and pH across hot-spring regions (Jia et al., 2014), and isoGMGT and brGMGT relative abundances follow contrasting trends in late Quaternary peat sequences (Tang et al., 2021).

Terrestrial brGMGT records provide further evidence of temperature sensitivity. Modern peat (Naafs et al., 2018) and lake datasets (Baxter et al., 2019) relate abundance and composition to temperature, and records from the Late Miocene Xining Basin and Plio-Pleistocene northern China reproduce regional cooling trends (Huang et al., 2024; Qian et al., 2025). In Xining, %brGMGTs provides a qualitative cooling signal, while compositional indices yield quantitative estimates (Huang et al., 2024). Calibration performance also depends on the temperature range and depositional setting. In cold northwestern Chinese peats, %brGMGTs and H-MBT′ perform poorly, and abundance screening improves calibration using warmer peat samples (Shen et al., 2025). In Lake Chala, long-term %brGMGT variability follows lake depth and mixing more closely than temperature (Baxter et al., 2024). These differences show how thermal responses interact with the habitats supplying brGMGTs to sediments.

The regional concentration contrast is consistent with a temperature influence. Median concentrations in the nearshore SCS cores exceed those in ECS surface sediments for both isoGMGTs (approximately 1.4 versus 0.4 ng g^{-1}) and brGMGTs (approximately 10 versus 4 ng g^{-1}; Fig. 2). Their enrichment in the warmer SCS provides qualitative regional support for enhanced GMGT production under warmer conditions. Sedimentary concentrations also integrate terrestrial supply, marine production, mineral dilution, and preservation, so the thermal contribution is best considered together with the source relationships established above.

The proposed association between GMGTs and anoxia has a different evidential basis. Putative archaeal Gms homologs were identified in obligately anaerobic taxa and oxygen-deficient metagenomes (Li et al., 2024), establishing an association between the detected biosynthetic potential and producer habitats. Demonstrating that oxygen depletion triggers GMGT synthesis requires experiments that manipulate oxygen availability in producing organisms. The radical SAM chemistry of Gms is also compatible in principle with activity in an oxygenated environment through intracellular reducing conditions, a possibility explicitly recognized in that study.

The coastal soils provide a complementary test of the environmental association. GDGT-0/CREN was below 2 in 15 of the 16 soils, and the sole sample above 2 (Station S4) had relatively low isoGMGT abundance. GDGT-0 is produced by several archaeal groups (Schouten et al., 2013), with ratios above 2 commonly associated with an enhanced anaerobic methanogenic lipid contribution (Blaga et al., 2008). The higher isoGMGT concentrations therefore occur among soils with comparatively weak methanogenic lipid signatures. The sedimentary isoGMGT distribution on the ECS shelf corroborates this interpretation: the co-eluting BHT-isomer signal reaches its maximum north of the Yangtze River mouth, away from the isoGMGTs/CREN maxima (Fig. S3c) (Yin et al., 2021), arguing against a simple hypoxia control on sedimentary isoGMGT abundance.

For brGMGTs, Lake Chala provides evidence of production in anoxic waters and surficial sediments (Baxter et al., 2021), with distinct water-column and sediment-associated components (Baxter et al., 2024). W07 extends this environmental comparison to an oxygenated marine water column: H1020a and H1020b peak at 75 m in both CL and TL fractions, supporting local production within oxygenated waters. Carbon isotope evidence for heterotrophic brGMGT sources in peats and lignites (Elling et al., 2023) further suggests that substrate availability can influence producing communities. These observations favor habitat-dependent controls on GMGT abundance and support brGMGT production in oxygenated as well as oxygen-deficient ecosystems. Anoxia may still enhance production or preservation in particular settings; the effect of oxygen availability on cellular GMGT yield remains an experimental question.

4.4. Marine H1020 variability and its paleoenvironmental significance

The simple offshore assemblage makes the relative contributions of H1020a and H1020b the principal measure of brGMGT compositional variability. Existing indices describe broader assemblages: brGMGTI combines several H1020 and H1034 components (Baxter et al., 2019),

H-MBT′ uses H1020c and H1034b in northern Chinese fluvial–lacustrine sediments (Qian et al., 2025), and IR_H (Hällberg et al., 2023) and the Riverine IndeX (Zhang et al., 2024) describe source-related compositional differences. In the offshore SCS samples, H1020a and H1020b together comprise more than 90% of brGMGTs, with H1020c detected in only some samples. We therefore use IR_{H1020} to summarize variation within this dominant marine pair.

The relationships with TEX_{86} differ between %brGMGTs and composition within the H1020 pair. For %brGMGTs, the pooled regression is positive ($R^2 = 0.274$, $p < 0.001$), SCS12 has a negative relationship ($R^2 = 0.246$, $p = 0.043$), and the remaining within-core fits are nonsignificant ($R^2 = 0.001–0.221$, $p = 0.090–0.912$; Fig. 9A). This contrast indicates a strong spatial component to the pooled association. The proportion of brGMGTs relative to brGDGTs integrates changes in both lipid pools, including terrestrial supply, as documented in the Bay of Bengal (Kirkels et al., 2022), and shifts in producer habitats associated with lake depth and mixing (Baxter et al., 2024; Wu et al., 2025).

IR_{H1020} shows a consistent inverse relationship with the published TEX_{86} index (Kim et al., 2010; Schouten et al., 2013) within all three offshore cores: SCS82 ($R^2 = 0.564$, $p = 0.002$), SCS73 ($R^2 = 0.431$, $p = 0.008$), and SCS12 ($R^2 = 0.255$, $p = 0.039$; Fig. 9B). The nearshore cores show little association (SCS52: $R^2 = 0.040$, $p = 0.493$; SCS77: $R^2 = 0.001$, $p = 0.932$). Pooling the cores produces a positive relationship ($R^2 = 0.314$, $p < 0.001$), consistent with offsets among sites. These regressions are therefore exploratory associations. Offshore stratigraphic changes thus share a common direction superimposed on different site baselines.

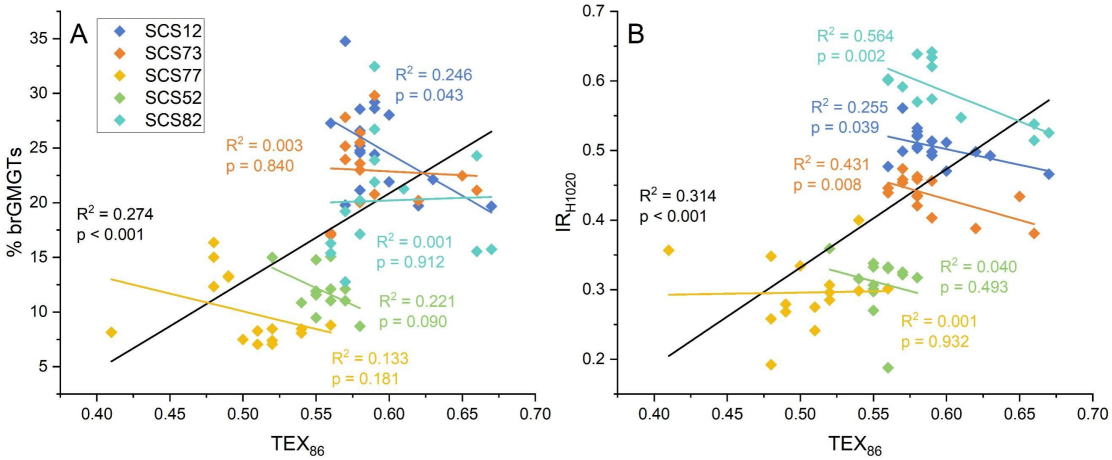


Fig. 9. Relationships between TEX_{86} and %brGMGTs (A) and IR_{H1020} (B) in the five SCS sediment cores. Colors distinguish individual cores. Colored lines represent within-core fits; black lines represent pooled fits. Reported R^2 and p values correspond to the respective fits. TEX_{86} data are from the published record (Zhou et al., 2026a); brGMGT indices are from this study.

Regional sedimentation rates and ages from nearby published records provide an approximate age context for SCS12, SCS73, and SCS82. Within this approximate age context,

the upward increase in TEX_{86} is consistent with regional glacial-to-interglacial warming (Fig. 10). IR_{H1020} generally decreases upward, indicating a reduced H1020b contribution as TEX_{86} increases. The shared direction across the three cores suggests that marine brGMGT composition may have responded to environmental changes accompanying the last glacial–interglacial transition.

The dominance of H1020a and H1020b throughout these records, together with their occurrence in W07 particles, is consistent with a marine lipid pool. This compositional continuity favors changes within marine producing communities as an explanation for the recurring offshore signal. The nearshore cores, which contain variable terrestrial contributions, show a different relationship with TEX_{86}.

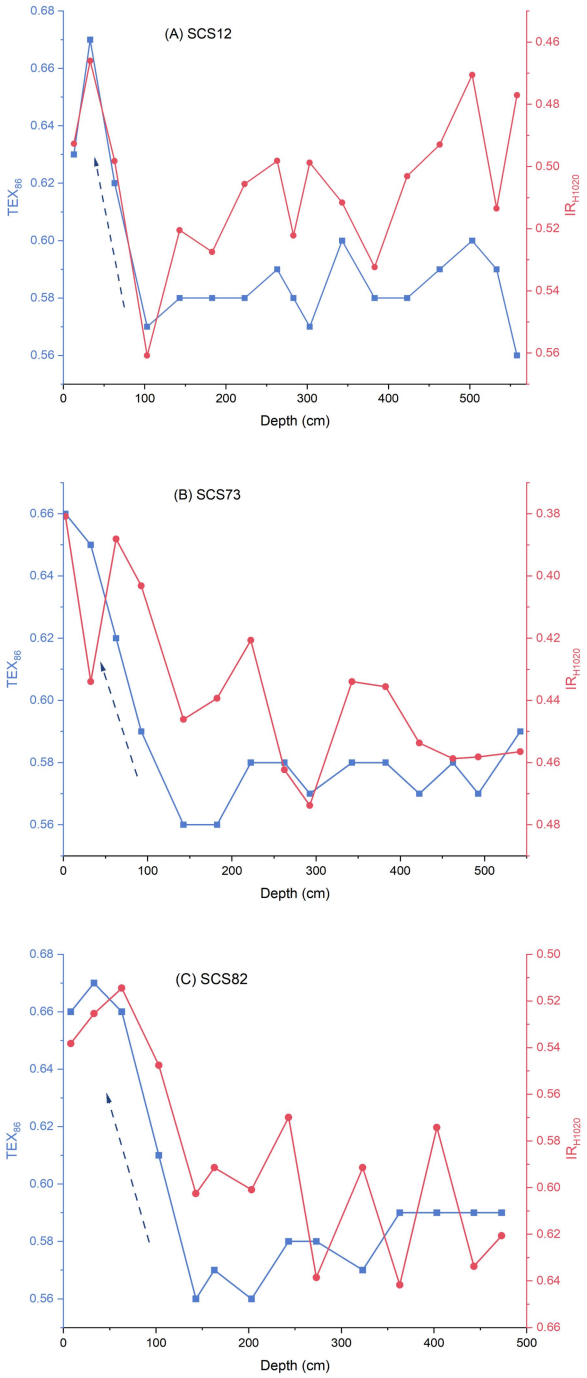


Fig. 10. TEX_{86} (blue) and IR_{H1020} (red) profiles in offshore SCS cores (A) SCS12, (B) SCS73, and (C) SCS82. The IR_{H1020} axes are reversed and have different ranges. IR_{H1020} is from this study. Regional sedimentation rates and nearby dated records suggest an approximate last-glacial-to-present context; the profiles are shown against sediment depth. Arrows indicate the approximate direction of glacial-to-interglacial warming.

Both thermal responses and shifts in producing communities could generate the recurring offshore pattern. Compositional changes associated with salinity in estuaries (Zhang et al., 2024) and with temperature and mixing in lakes (Baxter et al., 2019; Wu et al., 2025) demonstrate the sensitivity of brGMGT assemblages to habitat conditions. Evidence for heterotrophic sources (Elling et al., 2023) also makes organic substrate availability relevant.

During a glacial–interglacial transition, changes in temperature, water-column structure, and substrate supply could alter cellular H1020a/b composition, the relative abundance of its producers, or both.

IR_{H1020} thus describes recurring marine brGMGT compositional changes that may be associated with glacial–interglacial environmental variability. Its specific thermal or ecological significance remains unresolved. Establishing that relationship requires independent core chronologies and observations linking H1020a/b composition to marine producer habitats and hydrographic conditions.

5. Conclusions

Coastal soils contain an isoGMGT pool that can supply adjacent shelf sediments. The offshore decline in isoGMGTs/CREN and its high values near the Yangtze River mouth and Hangzhou Bay resemble published R_{soil} distributions, supporting its use as an indicator of relative soil organic matter input. Differences from other terrestrial biomarkers are consistent with the distinct organic matter components they represent.

BrGMGTs show a contrasting source pattern. Soils contain nine resolved peaks, including three H1048 components, whereas offshore sediments and quantifiable W07 particle assemblages are dominated by H1020a and H1020b. Their compositional agreement and subsurface concentration maximum support marine water-column production under oxygenated conditions. Together with the soil isoGMGT observations, these results favor an interpretation of GMGT distributions that incorporates producer habitats and organic matter sources alongside temperature and oxygen availability.

IR_{H1020} summarizes variation within the dominant marine H1020 pair. Its inverse relationships with TEX_{86} and consistent downcore trends in three offshore cores suggest sensitivity to environmental variability within an approximate last-glacial-to-present context. These records establish a marine compositional signal for further evaluation against independently dated changes in temperature, hydrography, and microbial ecology.

Acknowledgments

We thank the captains and crews of the NORC2025-03 cruise, supported by the National Natural Science Foundation of China, and the German R/V SONNE SO269 cruise.

L.D. is supported by the National Key Research and Development Program of China (Grant 2022YFC2805403), National Natural Science Foundation of China (Grant 42472370 and

W2511038), Shanghai Jiao Tong University 2030 Initiative (Grant WH510244001), State Key Laboratory of Submarine Geoscience (SGLabZZKT2025-09), the project “Ocean Negative Carbon Emission (ONCE)” and “Global Subseafloor Ecosystem and Sustainability (GSES)”. JJW received funding from the BMBF for the SO269-SOCLIS cruise (FKZ 03G0269), which was part of the Sino-German MEGAPOL project (FKZ 03F0786A). Q.L. is supported by the National Natural Science Foundation of China (Grant 42276087), the Guangdong Basic and Applied Basic Research Foundation (Grant 2019B030302004), the Marine Geological Survey Program of China Geological Survey (Grant DD20230065).

Conflict of Interest

The authors declare no conflicts of interest relevant to this study.

References

Baxter, A.J., Hopmans, E.C., Russell, J.M. and Sinninghe Damsté, J.S. (2019) Bacterial GMGTs in East African lake sediments: Their potential as palaeotemperature indicators. Geochimica et Cosmochimica Acta 259, 155-169.

Baxter, A.J., Peterse, F., Verschuren, D. and Sinninghe Damsté, J.S. (2021) Anoxic in situ production of bacterial GMGTs in the water column and surficial bottom sediments of a meromictic tropical crater lake: Implications for lake paleothermometry. Geochimica et Cosmochimica Acta 306, 171-188.

Baxter, A.J., Peterse, F., Verschuren, D. and Sinninghe Damsté, J.S. (2024) Assessment of branched glycerol monoalkyl glycerol tetraether (brGMGT)-based paleothermometry in the 250,000-year sediment record of Lake Chala, equatorial East Africa. Organic Geochemistry 195, 104812.

Blaga, C.I., Reichart, G.-J., Heiri, O. and Sinninghe Damsté, J.S. (2008) Tetraether membrane lipid distributions in water-column particulate matter and sediments: a study of 47 European lakes along a north–south transect. Journal of Paleolimnology 41, 523-540.

Sinninghe Damsté, J.S., Schouten, S., Hopmans, E.C., van Duin, A.C. and Geenevasen, J.A. (2002) Crenarchaeol: the characteristic core glycerol dibiphytanyl glycerol tetraether membrane lipid of cosmopolitan pelagic crenarchaeota. J Lipid Res 43, 1641-1651.

De Jonge, C., Hopmans, E.C., Zell, C.I., Kim, J.-H., Schouten, S. and Sinninghe Damsté, J.S. (2014) Occurrence and abundance of 6-methyl branched glycerol dialkyl glycerol tetraethers in soils: Implications for palaeoclimate reconstruction. Geochimica et Cosmochimica Acta 141, 97-112.

De Jonge, C., Stadnitskaia, A., Hopmans, E.C., Cherkashov, G., Fedotov, A., Streletskaya, I.D., Vasiliev, A.A. and Sinninghe Damsté, J.S. (2015) Drastic changes in the distribution of branched tetraether lipids in suspended matter and sediments from the Yenisei River and Kara Sea (Siberia): Implications for the use of brGDGT-based proxies in coastal marine sediments. Geochimica et Cosmochimica Acta 165, 200-225.

Dong, L., Li, Z. and Jia, G. (2019) Archaeal ammonia oxidation plays a part in late Quaternary nitrogen cycling in the South China Sea. Earth and Planetary Science Letters 509, 38-46.

Dong, L., Zhang, X., Jia, G., Du, Y., Li, L. and Li, Q. (2020) CO2-Induced Decoupling of Tropical Surface and Thermocline Water Temperature at the Onset of Interglacials. Geophysical Research Letters 47.

Eglinton, T.I. and Eglinton, G. (2008) Molecular proxies for paleoclimatology. Earth and Planetary Science Letters 275, 1-16.

Elling, F.J., Kattein, L., Naafs, B.D.A., Lauretano, V. and Pearson, A. (2023) Heterotrophic origin and diverse sources of branched glycerol monoalkyl glycerol tetraethers (brGMGTs) in peats and lignites. Organic Geochemistry 178, 104558.

Garcia, A.A., Chadwick, G.L., Liu, X.L. and Welander, P.V. (2024) Identification of two archaeal GDGT lipid-modifying proteins reveals diverse microbes capable of GMGT biosynthesis and modification. Proc Natl Acad Sci U S A 121, e2318761121.

Hällberg, P.L., Schenk, F., Jarne-Bueno, G., Schankat, Y., Zhang, Q., Rifai, H., Phua, M. and Smittenberg, R.H. (2023) Branched GDGT source shift identification allows improved reconstruction of an 8,000-year warming trend on Sumatra. Organic Geochemistry 186, 104702.

Hedges, J.I. and Mann, D.C. (1979) The characterization of plant tissues by their lignin oxidation products. Geochimica et Cosmochimica Acta 43, 1803-1807.

Huang, Y., Chen, C., Bai, Y., Fang, X., Song, L. and Li, Y. (2024) Late Miocene cooling and uplift recorded by bacterial H-GDGTs in the Xining Basin, northeastern Tibetan Plateau. Palaeogeography, Palaeoclimatology, Palaeoecology 650, 112354.

Huguet, C., Hopmans, E.C., Febo-Ayala, W., Thompson, D.H., Sinninghe Damsté, J.S. and Schouten, S. (2006) An improved method to determine the absolute abundance of glycerol dibiphytanyl glycerol tetraether lipids. Organic Geochemistry 37, 1036-1041.

Jia, C., Zhang, C.L., Xie, W., Wang, J.-X., Li, F., Wang, S., Dong, H., Li, W. and Boyd, E.S. (2014) Differential temperature and pH controls on the abundance and composition of H-GDGTs in terrestrial hot springs. Organic Geochemistry 75, 109-121.

Kim, J.-H., Schouten, S., Hopmans, E.C., Donner, B. and Sinninghe Damsté, J.S. (2008) Global sediment core-top calibration of the TEX86 paleothermometer in the ocean. Geochimica et Cosmochimica Acta 72, 1154-1173.
Kim, J.-H., van der Meer, J., Schouten, S., Helmke, P., Willmott, V., Sangiorgi, F., Koç, N., Hopmans, E.C. and Damsté, J.S.S. (2010) New indices and calibrations derived from the distribution of crenarchaeal isoprenoid tetraether lipids: Implications for past sea surface temperature reconstructions. Geochimica et Cosmochimica Acta 74, 4639-4654.
Kirkels, F.M.S.A., Usman, M.O. and Peterse, F. (2022) Distinct sources of bacterial branched GMGTs in the Godavari River basin (India) and Bay of Bengal sediments. Organic Geochemistry 167, 104405.
Li, Y., Yu, T., Feng, X., Zhao, B., Chen, H., Yang, H., Chen, X., Zhang, X.H., Anderson, H.R., Burns, N.Z., Zeng, F., Tao, L. and Zeng, Z. (2024) Biosynthesis of GMGT lipids by a radical SAM enzyme associated with anaerobic archaea and oxygen-deficient environments. Nat Commun 15, 5256.
Lincoln, S.A., Bradley, A.S., Newman, S.A. and Summons, R.E. (2013) Archaeal and bacterial glycerol dialkyl glycerol tetraether lipids in chimneys of the Lost City Hydrothermal Field. Organic Geochemistry 60, 45-53.
Liu, X.L., Summons, R.E. and Hinrichs, K.U. (2012) Extending the known range of glycerol ether lipids in the environment: structural assignments based on tandem mass spectral fragmentation patterns. Rapid Commun Mass Spectrom 26, 2295-2302.
Morii, H., Eguchi, T., Nishihara, M., Kakinuma, K., Konig, H. and Koga, Y. (1998) A novel ether core lipid with H-shaped C80-isoprenoid hydrocarbon chain from the hyperthermophilic methanogen Methanothermus fervidus. Biochim Biophys Acta 1390, 339-345.
Naafs, B.D.A., McCormick, D., Inglis, G.N. and Pancost, R.D. (2018) Archaeal and bacterial H-GDGTs are abundant in peat and their relative abundance is positively correlated with temperature. Geochimica et Cosmochimica Acta 227, 156-170.
Peterse, F., van der Meer, J., Schouten, S., Weijers, J.W.H., Fierer, N., Jackson, R.B., Kim, J.-H. and Sinninghe Damsté, J.S. (2012) Revised calibration of the MBT–CBT paleotemperature proxy based on branched tetraether membrane lipids in surface soils. Geochimica et Cosmochimica Acta 96, 215-229.
Qian, S., Yang, H., Wu, J., Xie, S. and Xu, Q. (2025) Assessing the reliability of H-brGDGTs as terrestrial paleothermometers in Plio-Pleistocene fluvio-lacustrine deposits from Northern China. Organic Geochemistry 208, 105046.
Raberg, J.H., Miller, G.H., Geirsdottir, A. and Sepulveda, J. (2022) Near-universal trends in brGDGT lipid distributions in nature. Sci Adv 8, eabm7625.
Schouten, S., Baas, M., Hopmans, E.C. and Sinninghe Damsté, J.S. (2008) An unusual isoprenoid tetraether lipid in marine and lacustrine sediments. Organic Geochemistry 39, 1033-1038.
Schouten, S., Hopmans, E.C., Schefuß, E. and Sinninghe Damsté, J.S. (2002) Distributional variations in marine crenarchaeotal membrane lipids: a new tool for reconstructing ancient sea water temperatures? Earth and Planetary Science Letters 204, 265-274.
Schouten, S., Hopmans, E.C. and Sinninghe Damsté, J.S. (2013) The organic geochemistry of glycerol dialkyl glycerol tetraether lipids: A review. Organic Geochemistry 54, 19-61.
Shen, Z., Zhao, M., Lin, T., Qu, X., Guo, H., Cao, J., Jia, G. and Rao, Z. (2025) Testing and improving brGMGTs-based paleotemperature estimates in peat sediments: Evidence from global surface peat samples and two well-dated Holocene peat cores in far Northwest China. Global and Planetary Change 245, 104700.
Summons, R.E., Welander, P.V. and Gold, D.A. (2022) Lipid biomarkers: molecular tools for illuminating the history of microbial life. Nat Rev Microbiol 20, 174-185.
Tang, X., Naafs, B.D.A., Pancost, R.D., Liu, Z., Fan, T. and Zheng, Y. (2021) Exploring the Influences of Temperature on "H-Shaped" Glycerol Dialkyl Glycerol Tetraethers in a Stratigraphic Context: Evidence From Two Peat Cores Across the Late Quaternary. Frontiers in Earth Science 8, 541685.
Tierney, J.E. and Tingley, M.P. (2015) A TEX(8)(6) surface sediment database and extended Bayesian calibration. Sci Data 2, 150029.

Tourte, M., Schaeffer, P., Grossi, V. and Oger, P.M. (2022) Membrane adaptation in the hyperthermophilic archaeon Pyrococcus furiosus relies upon a novel strategy involving glycerol monoalkyl glycerol tetraether lipids. Environ Microbiol 24, 2029-2046.

Weijers, J.W.H., Schouten, S., van den Donker, J.C., Hopmans, E.C. and Sinninghe Damsté, J.S. (2007) Environmental controls on bacterial tetraether membrane lipid distribution in soils. Geochimica et Cosmochimica Acta 71, 703-713.

Wu, J., Kou, Q., Shen, C., Wang, X., Zhu, L., Yang, H. and Xie, S. (2025) Dominant environmental variables affecting brGMGT-derived temperature proxies differ in lake surface sediments and sediment cores. Geochimica et Cosmochimica Acta 411, 71-85.

Xiao, W., Wang, Y., Zhou, S., Hu, L., Yang, H. and Xu, Y. (2016) Ubiquitous production of branched glycerol dialkyl glycerol tetraethers (brGDGTs) in global marine environments: a new source indicator for brGDGTs. Biogeosciences 13, 5883-5894.

Xie, S., Liu, X.-L., Schubotz, F., Wakeham, S.G. and Hinrichs, K.-U. (2014) Distribution of glycerol ether lipids in the oxygen minimum zone of the Eastern Tropical North Pacific Ocean. Organic Geochemistry 71, 60-71.

Yin, M., Duan, L., Song, J., Zhang, N., Li, X., Yuan, H. and Peng, Q. (2021) Bacteriohopanepolyols signature in sediments of the East China Sea and its indications for hypoxia and organic matter sources. Organic Geochemistry 158, 104268.

Zhang, Z.-X., Parlanti, E., Anquetil, C., Morelle, J., Laverman, A.M., Thibault, A., Bou, E. and Huguet, A. (2024) Environmental controls on the distribution of brGDGTs and brGMGTs across the Seine River basin (NW France): implications for bacterial tetraethers as a proxy for riverine runoff. Biogeosciences 21, 2227-2252.

Zhou, J. and Dong, L. (2024a) Molecular dynamics simulations reveal methylation in Me-GDGTs as a microbial low-temperature adaptation. Chemical Geology 644, 121844.

Zhou, J. and Dong, L. (2024b) Structural insights linking H-bridging of archaeal GDGTs to high temperature. Sci Total Environ 945, 174120.

Zhou, J. and Dong, L. (2025) Structural characterization of archaeal GDGT cyclization: Linking physiological adaptation to paleotemperature reconstruction. Earth and Planetary Science Letters 657, 119293.

Zhou, J., He, C., Jing, Y., Chen, Y., Waniek, J.J., Wang, F. and Dong, L. (2026a) Archaeal GMGTs in Marine Sediments as Potential Indicators of Terrestrial Input. Journal of Geophysical Research: Biogeosciences 131, e2026JG009966.

Zhou, J., Kang, D., Chen, S. and Dong, L. (2026b) Machine learning-based paleobathymetric reconstructions using archaeal lipid biomarkers. Sci Adv 12, eadz3284.

Zhou, J., Zhao, J., Wang, Y., Tong, Z., Wang, H., Guo, B., Deng, L., Wang, F., Liang, Q. and Dong, L. (2026c) Subsurface Production of Marine Derived Bacterial Tetraether Lipids: Implications for Paleoceanographic Reconstruction. Geophysical Research Letters 53, e2026GL122198.

Zhu, C., Talbot, H.M., Wagner, T., Pan, J.-M. and Pancost, R.D. (2011a) Distribution of hopanoids along a land to sea transect: Implications for microbial ecology and the use of hopanoids in environmental studies. Limnology and Oceanography 56, 1850-1865.

Zhu, C., Weijers, J.W.H., Wagner, T., Pan, J.-M., Chen, J.-F. and Pancost, R.D. (2011b) Sources and distributions of tetraether lipids in surface sediments across a large river-dominated continental margin. Organic Geochemistry 42, 376-386.

691

Contrasting terrestrial and marine sources of isoprenoid and branched glycerol monoalkyl glycerol tetraethers in marine sediments

Jiaming Zhou[1]#, Jiale Liu[1]#, Xinming Yuan[1], Chenxi He[1], Lingjun Li[1], Yunru Chen[2], Binbin Guo[3], Zian Tong[1], Joanna J. Waniek[4], Yanwei Wang[1], Jing Zhao[3], Longhui Deng[1], Fengping Wang[1], Qianyong Liang[3], Liang Dong[1]*

[1] State Key Laboratory of Submarine Geoscience; Key Laboratory of Polar Ecosystem and Climate Change, Ministry of Education; Shanghai Key Laboratory of Polar Life and Environment Sciences; and School of Oceanography, Shanghai Jiao Tong University, 1954 Huashan Road, Shanghai 200030, China.

[2] MARUM–Center for Marine Environmental Sciences, University of Bremen, D-28359 Bremen, Germany.

[3] National Engineering Research Center of Gas Hydrate Exploration and Development, Guangzhou Marine Geological Survey, China Geological Survey, Guangzhou, 511457, China

[4] Leibniz Institute for Baltic Sea Research, Warnemünde, Rostock 18119, Germany.

#These authors contributed equally.

Corresponding author: Liang Dong (dongliang@sjtu.edu.cn).

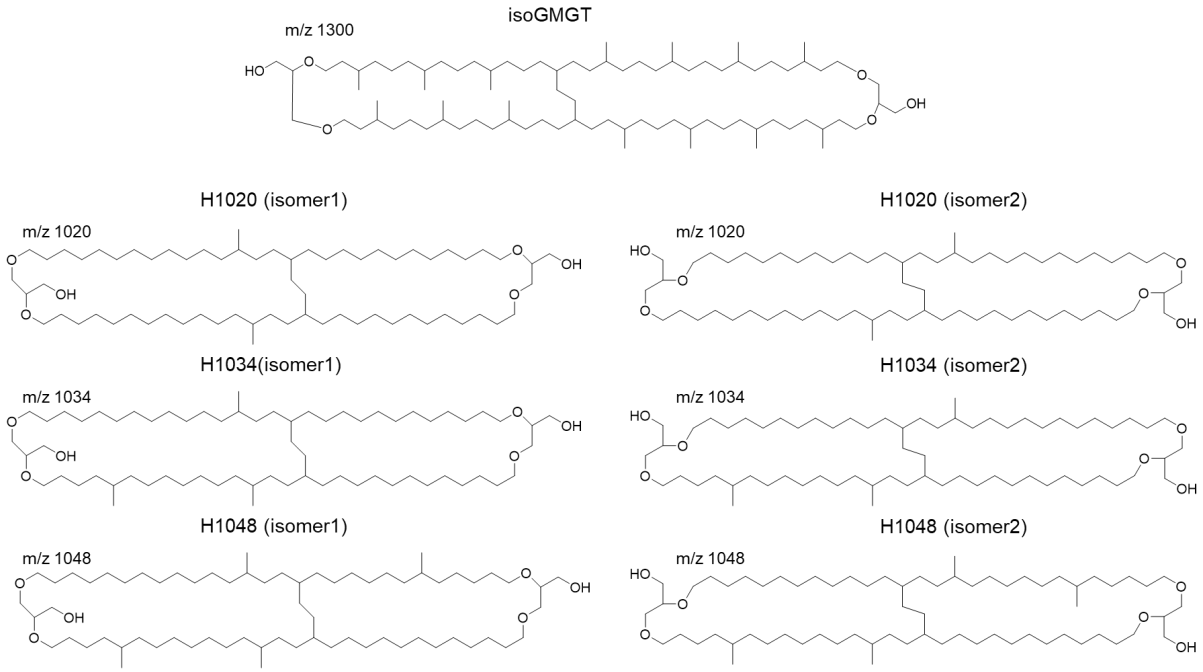
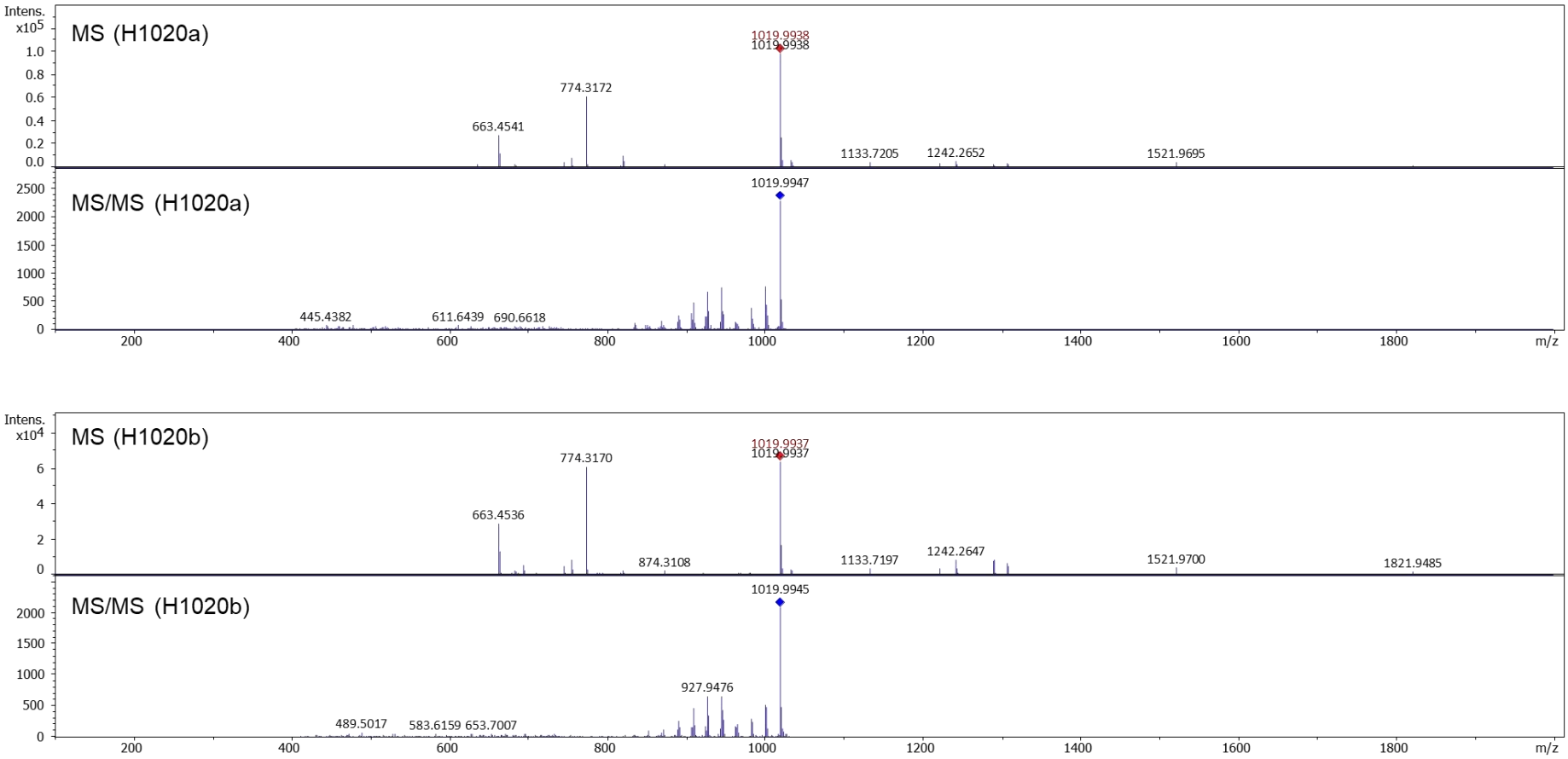
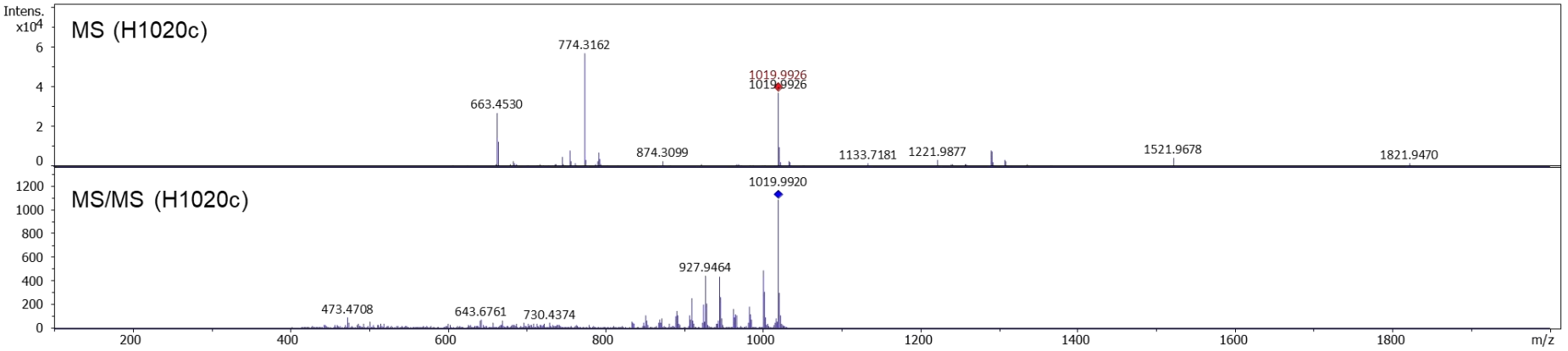
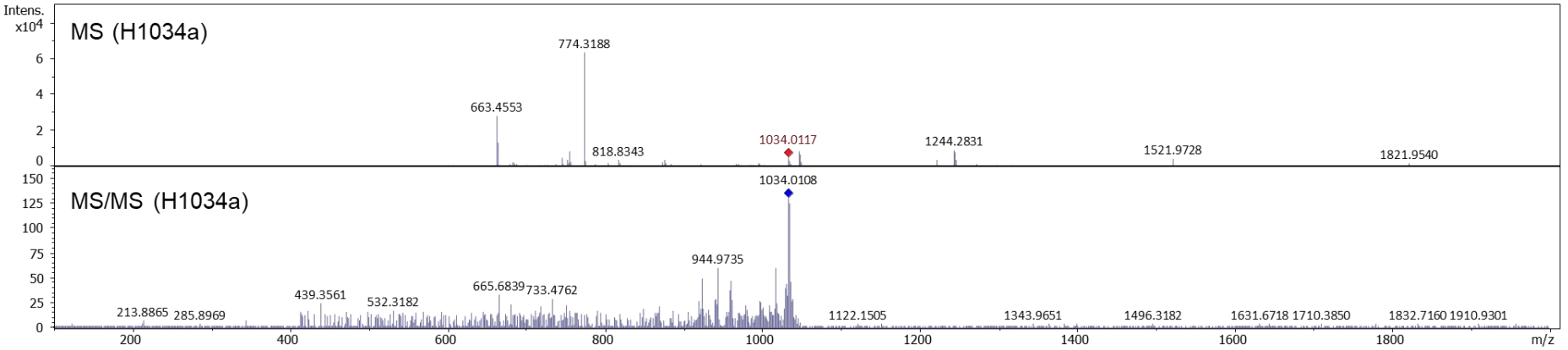
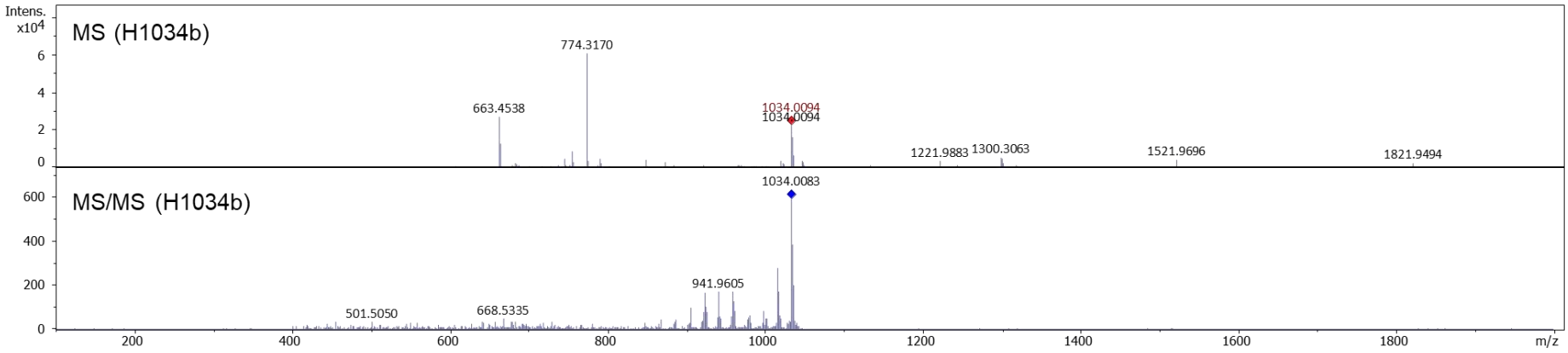


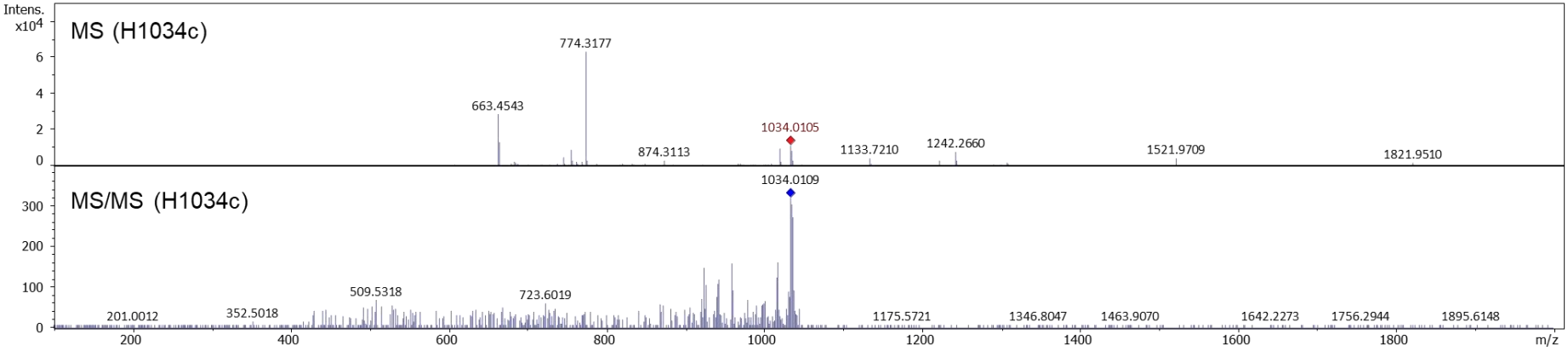
Figure S1. Schematic structure of isoGMGT-0 and hypothetical structures of brGMGTs. The two H1020 structures labelled isomer 1 and isomer 2 are based on the hypothetical models proposed by Baxter et al. (2019). The H1034 and H1048 structures are illustrative extensions of these models, containing one and two additional methyl groups, respectively. The positions of the additional methyl groups remain unresolved; possible methylation at C-5 and C-6 has been suggested by analogy with brGDGTs (Wu et al., 2025). The methyl-group positions shown here are illustrative and do not constitute structural assignments. The precise positions of the interchain linkages in brGMGTs also remain to be established. The labels isomer 1 and isomer 2 distinguish the schematic alternatives only and do not imply assignments to the chromatographic components a–c or represent all possible isomers.

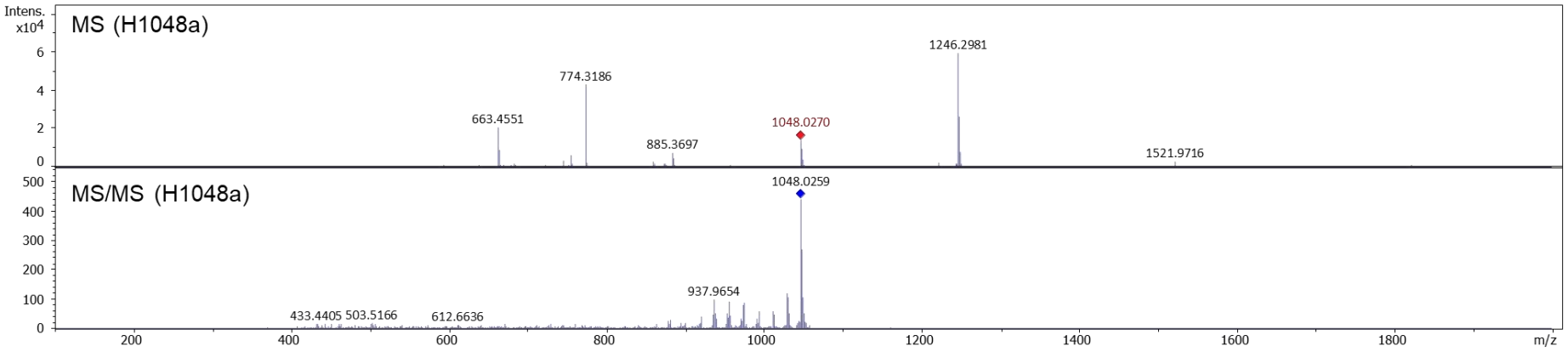

Intens.
x10^5
MS (H1020a)
1019.9938
1019.9938
774.3172
663.4541
1133.7205
1242.2652
1521.9695
MS/MS (H1020a)
1019.9947
445.4382
611.6439
690.6618
m/z
Intens.
x10^4
MS (H1020b)
1019.9937
1019.9937
774.3170
663.4536
874.3108
1133.7197
1242.2647
1521.9700
1821.9485
MS/MS (H1020b)
1019.9945
927.9476
489.5017
583.6159
653.7007
m/z

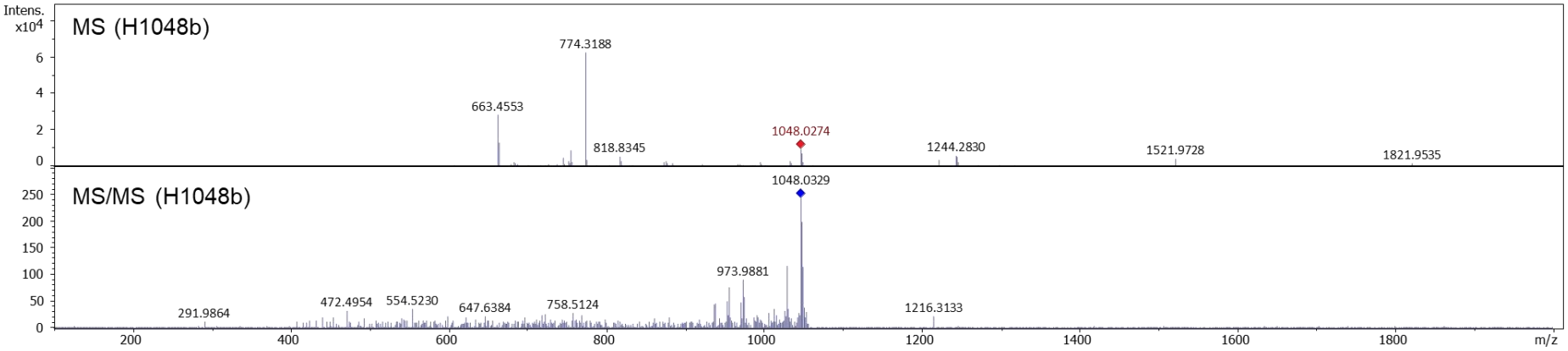

Intens.
x10^4
MS (H1020c)
774.3162
1019.9926
1019.9926
663.4530
874.3099
1133.7181
1221.9877
1521.9678
1821.9470
MS/MS (H1020c)
1019.9920
927.9464
473.4708
643.6761
730.4374
m/z


Intens.
x10^4
MS (H1034a)
774.3188
663.4553
818.8343
1034.0117
1244.2831
1521.9728
1821.9540
MS/MS (H1034a)
1034.0108
944.9735
665.6839
733.4762
439.3561
532.3182
213.8865
285.8969
1122.1505
1343.9651
1496.3182
1631.6718
1710.3850
1832.7160
1910.9301
m/z


Intens.
x10^4
MS (H1034b)
774.3170
663.4538
1034.0094
1034.0094
1221.9883
1300.3063
1521.9696
1821.9494
MS/MS (H1034b)
1034.0083
941.9605
501.5050
668.5335
m/z


Intens.
x10^4
MS (H1034c)
774.3177
663.4543
1034.0105
874.3113
1133.7210
1242.2660
1521.9709
1821.9510
MS/MS (H1034c)
1034.0109
509.5318
723.6019
201.0012
352.5018
1175.5721
1346.8047
1463.9070
1642.2273
1756.2944
1895.6148
m/z


Intens.
x10^4
MS (H1048a)
1246.2981
774.3186
663.4551
1048.0270
885.3697
1521.9716
MS/MS (H1048a)
1048.0259
937.9654
433.4405
503.5166
612.6636
m/z


Intens.
x10^4
MS (H1048b)
774.3188
663.4553
1048.0274
818.8345
1244.2830
1521.9728
1821.9535
MS/MS (H1048b)
1048.0329
973.9881
291.9864
472.4954
554.5230
647.6384
758.5124
1216.3133
m/z

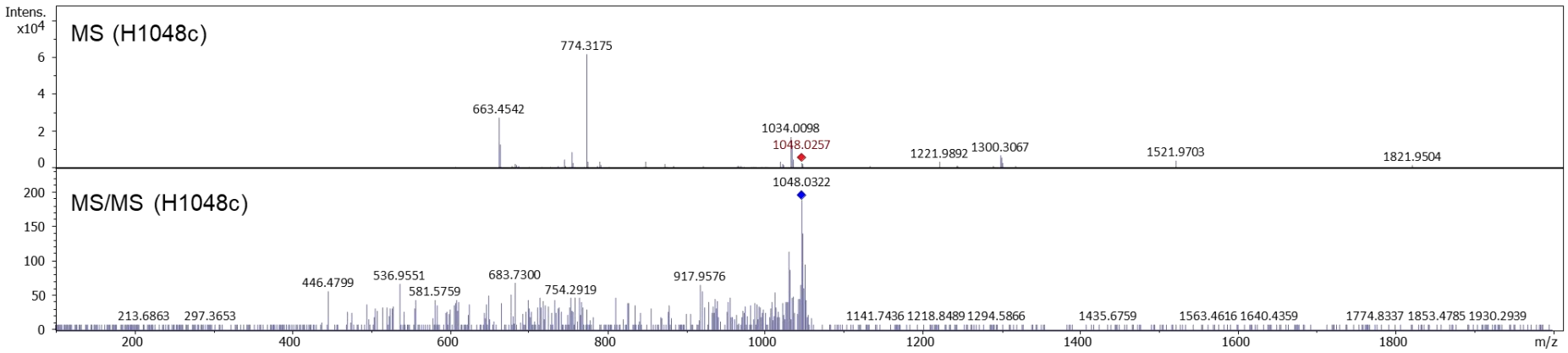


Figure S2. Full-scan (MS) and tandem (MS/MS) mass spectra of the nine chromatographically resolved brGMGT components (H1020a–c, H1034a–c, and H1048a–c), acquired by LC–APCI–QTOF–MS in positive-ion mode. For each component, the upper and lower panels show the full-scan and product-ion spectra, respectively. The protonated precursor ions ($[M+H]^+$) occur at nominal m/z 1020, 1034, and 1048 for the corresponding homologues.

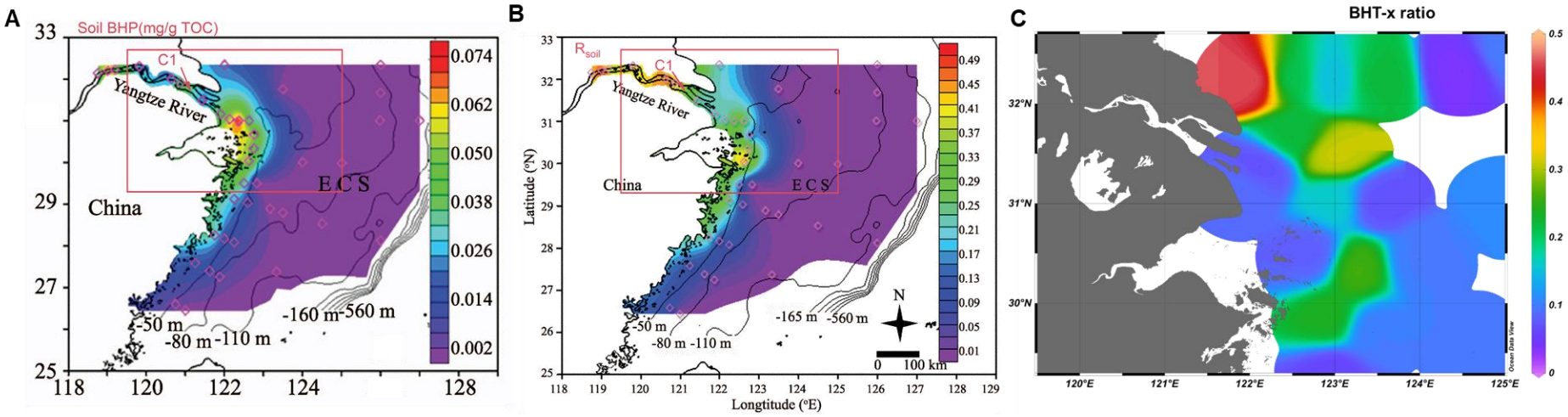


Figure S3. Published distributions of bacteriohopanepolyol (BHP) indicators in surface sediments of the Yangtze River Estuary and East China Sea. (A) Soil-marker BHP concentrations (mg g^{-1} TOC) and (B) the soil organic matter index Rsoil, adapted from Zhu et al. (2011). Rsoil expresses soil-marker BHPs relative to their sum with bacteriohopanetetrol. The red boxes were added here to outline the approximate area of the present study(Fig. 3). (C) The BHT-x ratio, a sedimentary marker of marine hypoxia and anammox, plotted using data from Yin et al. (2021).

References

Baxter, A.J., Hopmans, E.C., Russell, J.M. and Sinninghe Damsté, J.S. (2019) Bacterial GMGTs in East African lake sediments: Their potential as palaeotemperature indicators. Geochimica et Cosmochimica Acta 259, 155-169.

Wu, J., Kou, Q., Shen, C., Wang, X., Zhu, L., Yang, H. and Xie, S. (2025) Dominant environmental variables affecting brGMGT-derived temperature proxies differ in lake surface sediments and sediment cores. Geochimica et Cosmochimica Acta 411, 71-85.

Yin, M., Duan, L., Song, J., Zhang, N., Li, X., Yuan, H. and Peng, Q. (2021) Bacteriohopanepolyols signature in sediments of the East China Sea and its indications for hypoxia and organic matter sources. Organic Geochemistry 158.

Zhu, C., Talbot, H.M., Wagner, T., Pan, J.-M. and Pancost, R.D. (2011) Distribution of hopanoids along a land to sea transect: Implications for microbial ecology and the use of hopanoids in environmental studies. Limnology and Oceanography 56, 1850-1865.